 doi:10.20944/preprints202009.0720.v1

A Perspective on Cell Tracking with Magnetic Particle Imaging

Olivia C Sehl[1,2], Julia J Gevaert[1,2], Kierstin P Melo[1,2], Natasha N Knier[1,2], and Paula J Foster[1,2]

[1]Robarts Research Institute, Western University, London, Ontario, Canada
[2]Department of Medical Biophysics, Western University, London, Ontario, Canada

 doi:10.20944/preprints202009.0720.v1

Abstract

Magnetic Particle Imaging (MPI) is a new imaging modality that sensitively and specifically detects superparamagnetic iron oxide nanoparticles (SPIONs). Many labs have been developing cellular magnetic resonance imaging (MRI) tools using both SPIONs and fluorine-19 (19F)-based contrast agents for numerous important applications, including tracking of immune and stem cells used for cellular therapies. SPION-based MRI cell tracking has very high sensitivity, but low specificity. SPIONs produce negative contrast in MRI, or signal voids. SPIO is not directly detected by MRI, but indirectly through its relaxation effects on protons, therefore, it is not possible to reliably quantify the local tissue concentration of SPION particles and cell number cannot be determined. 19F based cell tracking uses perfluorocarbons (PFC) to label cells. The number of 19F atoms can be directly measured from 19F MR images and related to cell number. 19F MRI has high specificity, but low sensitivity. MPI cell tracking displays great potential for overcoming the challenges of MRI-based cell tracking allowing for both high cellular sensitivity and high specificity and quantification of SPIO labeled cell number. In this paper we describe nanoparticle and MPI system factors that influence MPI sensitivity and resolution, quantification methods and give our perspective on testing and applying MPI for cell tracking.

Keywords: magnetic particle imaging, cell tracking

 doi:10.20944/preprints202009.0720.v1

In Vivo Cell Tracking

Cellular therapies are now recognized as effective medicines for treatment of a specific subset of cancers as well as a growing list of autoimmune, degenerative, genetic, and infectious diseases. Cell therapy refers to the administration of immune cells (such as T cells or dendritic cells) which are used to treat cancer, and stem cells (such as mesenchymal stem cells or pluripotent stem cells) which have numerous potential applications including treatment of amyotrophic lateral sclerosis, diabetes, graft versus host disease, kidney disease, liver disease, multiple sclerosis, myocardial disease, osteoarthritis, Parkinson's disease, spinal cord injury and stroke. Numerous cell therapy clinical trials are underway.

Despite the immense promise of cell therapies, clinical results have been highly variable because of variations in cell source, preparation, and route of administration/implantation methodology. Many critical questions about the presence, numbers, persistence, and delivery of cells remain unanswered. For example, in cancer immunotherapy, the magnitude of an anti-tumor response is proportional to the quantity of antigen presenting cells that reach a target lymph node, [1–3] and therefore, it is crucial to know whether the injected cells have migrated to the target, and how many. In stem cell therapy, the survival and persistence of cells at the implant site informs on whether a patient may need repeat dosing or other interventions. These types of questions must be answered to improve the safety and success of cell therapies and for it to realize its full potential. *In vivo* cellular imaging tools have the potential to answer these questions. The ideal imaging modality for monitoring cell therapies would be non-invasive, non-ionizing, sensitive enough to allow detection and quantification of a few hundred cells, specific and, importantly, quantitative - providing a measure of cell number.

MRI has been widely used for *in vivo* cell tracking. Cellular MRI uses contrast agents for labeling specific cells, thereby enhancing their detectability.[4,5] The most often used agents for cell tracking with MRI are magnetite (Fe_3O_4)-based superparamagnetic iron oxide nanoparticles (SPIONs). The presence of SPIONs in cells causes a distortion in the magnetic field and leads to abnormal signal hypo-intensities in iron-sensitive images.[4] Areas containing SPION-labeled cells therefore appear as regions of low signal intensity on MRI images, creating negative contrast. Therapeutic cell types including mesenchymal stem cells,[6,7] progenitor cells,[8] T-lymphocytes,[9] dendritic cells,[10,11] and pancreatic islets,[12,13] have been labeled with SPIONs and tracked with MRI. The iron label has minimal impact on cell function or phenotype at a wide range of iron loading

Preprints (www.preprints.org) | NOT PEER-REVIEWED | Posted: 29 September 2020 doi:10.20944/preprints202009.0720.v1

levels.[14] This technique is highly sensitive, permitting the imaging of single cells *in vivo*[15], under ideal conditions. There are, however, several limitations of iron-based MRI cell tracking. The first is low specificity due to other low-signal regions in MR images; such as the air-filled lungs or a region of hemorrhage. Although ultra-short echo time imaging methods have been developed for producing positive contrast from iron-labeled cells, these too have similar problems with specificity. Second, quantification of iron-induced signal loss is complicated since the measure of the signal void volume is not linear with the number of cells.

Fluorine-19 (^{19}F) MRI with perfluorocarbon (PFC) nanoemulsions to label cells has been also used for cell tracking.[16,17] ^{19}F cell tracking addresses some of the limitations associated with iron-based cell tracking. First, the ^{19}F signal is specific since endogenous ^{19}F is so low that there is not any appreciable tissue background signal. Second, in contrast to the indirect visualization of SPIOs by observed proton signal loss, the spins of ^{19}F nuclei are directly detected and image contrast is proportional to the number of ^{19}F nuclei per voxel. Cell number can be determined if a measurement of ^{19}F nuclei/cell is obtained by NMR spectroscopy; the ^{19}F signal intensity for the cells of interest is compared to the ^{19}F signal intensity of a reference tube containing a known ^{19}F concentration and the NMR calibration value.[18] The main limitation of ^{19}F cell tracking is low sensitivity; thousands of labeled cells per voxel are required. Fluorine sensitivity improves with higher field strengths and preclinical studies have reported *in vivo* detection of as few as 1000 cells per voxel.[19] However, the first human clinical trial at 3 Tesla (T) demonstrated a cellular detection limit between 1 and 10 million cells.[20]

Magnetic Particle Imaging (MPI) is a new imaging modality that directly detects SPIONs.[21,22] MPI is built around a gradient magnet system. Two opposing electromagnets form strong gradient magnetic fields (in the order of T), and a field free region (FFR) is created in the position where these gradient fields cancel out. The gradient field (also known as the selection field) saturates the magnetization of all SPIONs except for those SPIONs at the FFR, which experience no magnetic field. The FFR is shifted over an imaging volume, by changing the current through the electromagnets, to produce an image. When the FFR traverses a location containing SPIONs, the SPIONs magnetization changes nonlinearly in response to a secondary sinusoidal excitation magnetic field (in the order of mT). This change in SPIO magnetization induces a voltage which is detected via a receiver coil, and the resulting signal can be assigned to the

Preprints (www.preprints.org) | NOT PEER-REVIEWED | Posted: 29 September 2020 doi:10.20944/preprints202009.0720.v1

instantaneous FFR location to reconstruct the final image.[23] The voltages induced are linearly proportional to the number of SPIONs at the FFR location, enabling quantification of SPIONs.

MPI cell tracking has the potential to address many of the limitations presented by SPION- and ^{19}F-based cell tracking. First, since the MPI signal is only generated when the magnetic moments of the SPIONs rotate in response to the applied fields there is no signal from tissue. This imbues MPI with a positive "hot-spot" contrast that provides spatial localization without ambiguity. Second, MPI has high sensitivity. MPI's sensitivity derives from the direct detection of the electronic magnetization of SPION, which is 10^8 times larger than the nuclear magnetization of protons seen in MRI.[24] Third, the MPI signal is linearly quantitative with SPION concentration, and therefore the number of SPION labeled cells can be calculated.[25] The shortcomings of MPI include relatively low spatial resolution, compared to MRI, and the requirement that anatomical images must be acquired separately with a different imaging modality. A comparison of MSC tracking with iron and ^{19}F based MRI and MPI is shown in Figure 1. For a detailed description of the physics of MPI readers are referred to review articles by Goodwill et al. (2012),[22] Zheng et al. (2017),[22] Yu et al. (2017)[26], Wu et al. (2019)[27] and Talebloo et al. (2020).[28]

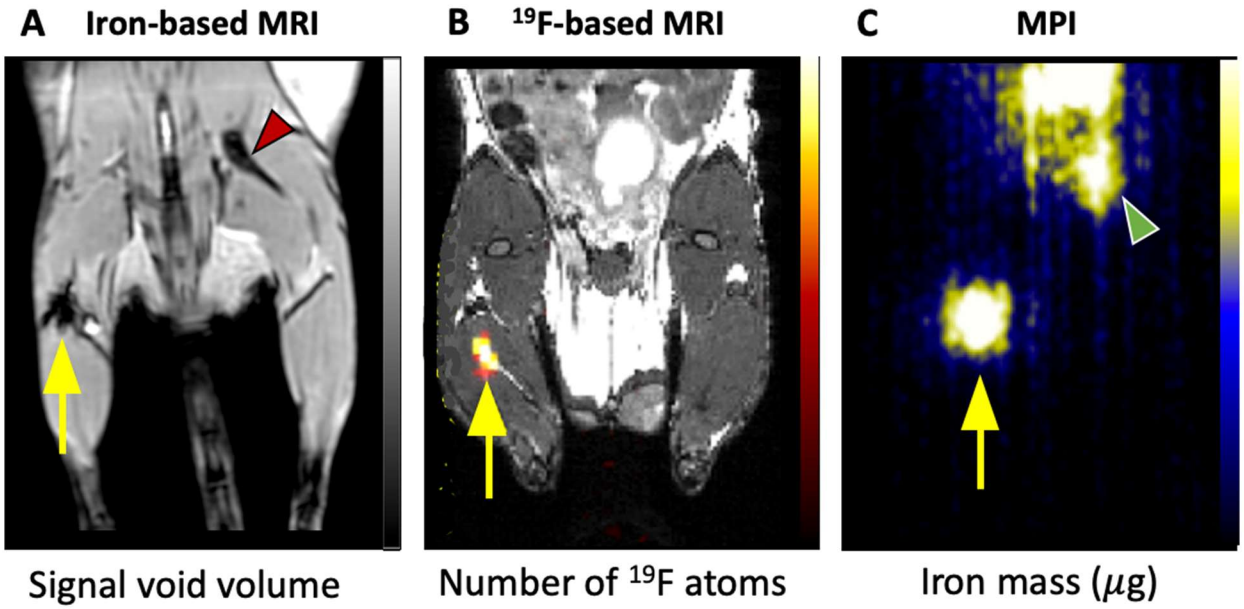

Figure 1 – A comparison of iron-based MRI, 19F-based MRI, and MPI for cell tracking. Mesenchymal stem cells (MSC) labeled with ferumoxytol **(A, C)** or perfluorocarbon **(B)** were implanted intramuscularly and imaged using 1H MRI **(A)**, 19F MRI with overlay to anatomical 1H **(B)**, or MPI **(C)**. The signal associated with MSC is denoted by the yellow arrows in each image. Quantitation of the signal is shown below as a measure of the signal void volume **(A)**, a measure of the number of 19F nuclei and associated number of MSC **(B)**, and a measure of the iron mass and associated number of MSC **(C)**. The red arrow **(A)** shows dark signal coming from the bone and this demonstrates the lack of specificity of iron-based MRI. Likewise, the green arrow **(C)** points to MPI signal generated from iron contamination in the mouse digestive system. Images reprinted from Sehl et al. Tomography 2019 **(A,C)** and Gaudet et al. Magnetic Resonance in Medicine 2017 **(B)**.

 doi:10.20944/preprints202009.0720.v1

MPI Sensitivity and Resolution

Particle sensitivity in MPI refers to the lowest mass of SPIO detected per imaging unit (e.g., ug/mm3). For MPI cell tracking, the aim is to optimize the *cellular sensitivity*, which refers to the lowest number of SPION-labeled cells detected per imaging unit (i.e. number of cells/mm^3). The sensitivity of MPI depends on both nanoparticle and scanner specific factors. Nanoparticle factors include the strength of the nanoparticle magnetization (stonger magnetization improves MPI signal), the rate of SPION relaxation at the FFR, and the efficiency of the nanoparticle cell labeling (more iron per cell leads to higher sensitivity). Scanner specific factors include increasing the amplitude of the excitation field,[29] decreasing the gradient strength (at the cost of resolution), and signal averaging. For example, increasing the overlap fraction or combining multiple projections (*i.e.* 3D imaging) can improve cell detection. An important consideration is that cellular sensitivity *in vitro* may be enhanced compared to when cells are *in vivo*. This is due to dispersion of cells from the site of administration and additional factors such as breathing motion.

The current *in vitro* detection limit is reported at 200 stem cells labeled with ferucarbotran (1000 cells imaged with SNR = 5),[30] however these MPI cellular detection limits should be demonstrated and evaluated more closely. Song et al.[31] reports an *in vivo* cell detection limit of 250 HeLa cells injected subcutaneously in a bolus and using a custom MPI SPION (refered to as the Janus nanoparticle). There is no doubt that cellular sensitivity will improve with further advances in acquisition strategies and SPION design.

The resolution of MPI is driven primarily by SPION relaxation. *Neel relaxation* refers to the reversal of the SPION magnetic moment whereas *Brownian relaxation* refers to the physical rotation of the SPION, in response to the excitation magnetic field used in MPI. [32–34] The dominant relaxation mechanism depends primarily on the SPION size and the MPI resolution worsens with increasing Brownian relaxation. Theoretical modeling based upon the Langevin theory of SPIONs predicts that resolution improves with increasing core size. However, Tay *et al.*[33] have found that improved resolution with increasing magnetic core size follows the steady-state prediction up to approximately 25 nm when the effects of SPION rotational times become significant due to increasing Brownian relaxation. SPIONs above this size range experience increased drag, slowing their magnetization response and limiting resolution. Importantly, this work looked at single core mono-dispersed nanoparticles. Many of the SPIONs used for cell tracking are multi-domain, clustering nanoparticles with more complicated physics.

 doi:10.20944/preprints202009.0720.v1

Resolution is also influenced by the interaction of the nanoparticle and the magnetic field gradient. Stronger gradients increase resolution but at the cost of sensitivity. The spatial resolution of MPI using currently available SPIONs is approximately 1 mm[25] and using optimized iron oxide nanoparticles, MPI resolution of 200 μm has been demonstrated.[35] With further development, sensitivity and resolution should increase and significant improvements to cell detection limits will be possible.

SPIONs for MPI

As described above, both MPI sensitivity and resolution are closely related to the type of SPION, however the ideal SPIONs for MPI are still not known. In early MPI cell tracking, commercially available SPIONs used for MRI were evaluated, including ferucarbotran (Resovist, now manufactured as Vivotrax^{TM}, Magnetic Insight Inc.), and ferumoxtyol. Ferucarbotran has improved MPI characteristics compared to ferumoxytol[36–38], and ferucarbotran has been used in MPI studies of mice to detect mesenchymal stem cells,[36,39] neural stem cells,[40] neural progenitor cells,[30] pancreatic islets,[13] T-cells,[9] and macrophages.[38,41] Although widely used, ferucarbotran is no longer considered optimal for MPI because it has a bimodal size distribution, predominantly containing small cores ~ 5 nm in diameter (70%) with a small fraction (30%) of multi-core aggregates with an effective size of 24 nm.[42] The individual cores are too small to magnetize significantly and so the MPI signal predominately originates from the clustered multi-core structures. Optimizing SPIONs expressly for MPI is emerging as a powerful area of research and will be critical for improving sensitivity and spatial resolution.[33] Approaches to improve MPI sensitivity include increasing the fraction of these larger aggregates[42] or by fractionation of ferucarbotran.[43] Lastly, the synthesis of homogeneously distributed single-core SPIONs with optimized core diameters is being investigated.[44]

MPI relaxometry is commonly used as a first step to characterize SPIONs. MPI relaxometry measures the net magnetization of SPIONs, by turning off the selection field and applying a negative magnetic field then a positive field, and back. SPIONs in a sample are driven from a negative magnetic saturation to positive, and vice versa. The output is the derivative of the Langevin function, also called the point spread function (PSF). The signal intensity, or height, of the PSF reflects the sensitivity of the SPION. The full-width half maximum (FWHM) relates to the spatial resolution of the SPION.[45] A narrower tracer response indicates superior spatial

Preprints (www.preprints.org) | NOT PEER-REVIEWED | Posted: 29 September 2020 doi:10.20944/preprints202009.0720.v1

resolution and a greater signal intensity per mass of iron indicates superior sensitivity. We have evaluated several commercially available SPIONs (Figure 2). In our experience relaxometry has significant value for testing SPIONs prior to use for MPI as certain SPIONs that may not, in theory, seem suitable for MPI show surprisingly good sensitivity (ie. micron-sized superparamagnetic polystrene beads, MPIO).

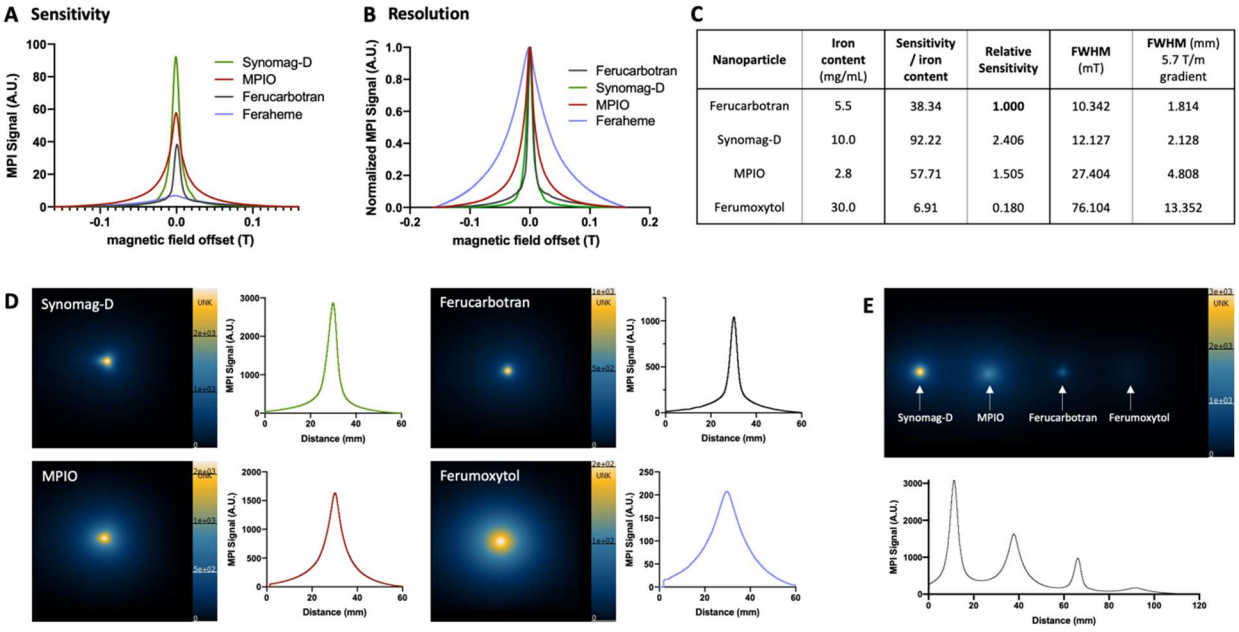

Nanoparticle	Iron content (mg/mL)	Sensitivity / iron content	Relative Sensitivity	FWHM (mT)	FWHM (mm) 5.7 T/m gradient
Ferucarbotran	5.5	38.34	**1.000**	10.342	1.814
Synomag-D	10.0	92.22	2.406	12.127	2.128
MPIO	2.8	57.71	1.505	27.404	4.808
Ferumoxytol	30.0	6.91	0.180	76.104	13.352

Figure 2 – A comparison of commercially available SPIONs using MPI relaxometry. PSFs show that the relative sensitivity of Synomag-D is superior to MPIO, ferucarbotran, and feraheme (in order) per gram of iron content **(A)**. Normalized PSFs show that the resolution (FWHM) of ferucarbotran is superior to synomag-D, MPIO, and feraheme (in order) **(B)**. Measurements of sensitivity and resolution for each nanoparticle is outlined in **(C)**. MPI of each individual SPION (30 ug) and the corresponding intensity profile is shown in **(D)**. A single MPI image and intensity profile of all four SPIONs (30 ug) show similar results **(E)**. MPI images are displayed in full-dynamic range. With the same iron content, each nanoparticle has different MPI characteristics. Defined acronyms: A.U. = arbitrary units, FWHM = full width half maximum, MPIO = micron-sized iron oxide.

For cell tracking with MPI it is also critical that the SPION of choice is taken up by cells effectively; not all SPIONs are. Effectively labeled cells have high intracellular iron load and low extracellular iron. High iron load is important for MPI sensitivity. Extracellular iron in cell samples can lead to overestimation of iron content measured by MPI, and *in vivo* extracellular iron can be taken up by host cells leading to lower specificity. The coating of SPIONs influences their interaction with the cell membrane and the mechanism of uptake. Most SPIONs have a carbohydrate coat, typically dextran or carboxydextran. The carboxyl groups associated with ferucarbotrans lead to a high affinity to the cell membrane.[46] Several other surface coating modification strategies[47] have been shown to enhance internalization of SPIONs.[48,49] Many cell

 doi:10.20944/preprints202009.0720.v1

types can be labeled *in vitro* simply by overnight incubation with SPIONs. However, for certain cell types (ie. immune cells) and certain SPIONs (ie. ferumoxytols[50,51]) co-incubation alone is not effective. Transfection agents (TAs) are commonly used to facilitate or enhance cellular incorporation of SPIONs into cells, including poly-L-lysine, lipofectamine and protamine sulfate (often with heparin).[52–54] TAs coat the surface of SPIONs and shuttle the SPION into the cell. This can lead to effective labeling of cells, increased iron content in cells or faster labeling. As demonstrated in Figure 3 A-C, the addition of protamine sulfate and heparin significantly improves uptake of ferucarbotran by mesenchymal stem cells. However, several studies have shown that SPION-TA complexes may clump cells together and can lead to higher amounts of free iron in cell preparations.[54] It is also necessary to test whether TAs alter cell functionality or phenotype. For example, certain TAs reduce the immunopotency of dendritic cells.[55] Importantly, we have recently observed that the MPI characteristics of SPIONs are altered by TAs. Figure 3C-G compares the MPI sensitivity and resolution of samples of ferucarbotran and ferucarbotran mixed with protamine sulfate/heparin. The addition of the TA leads to lower MPI signal and lower resolution images. This requires more study but may result from altered relaxation characteristics due to clustering of cells and iron cores. Therefore, while TAs may be used to achieve higher intracellular iron with the goal of improving MPI sensitivity, this gain may be counteracted by this effect.

Preprints (www.preprints.org) | NOT PEER-REVIEWED | Posted: 29 September 2020 doi:10.20944/preprints202009.0720.v1

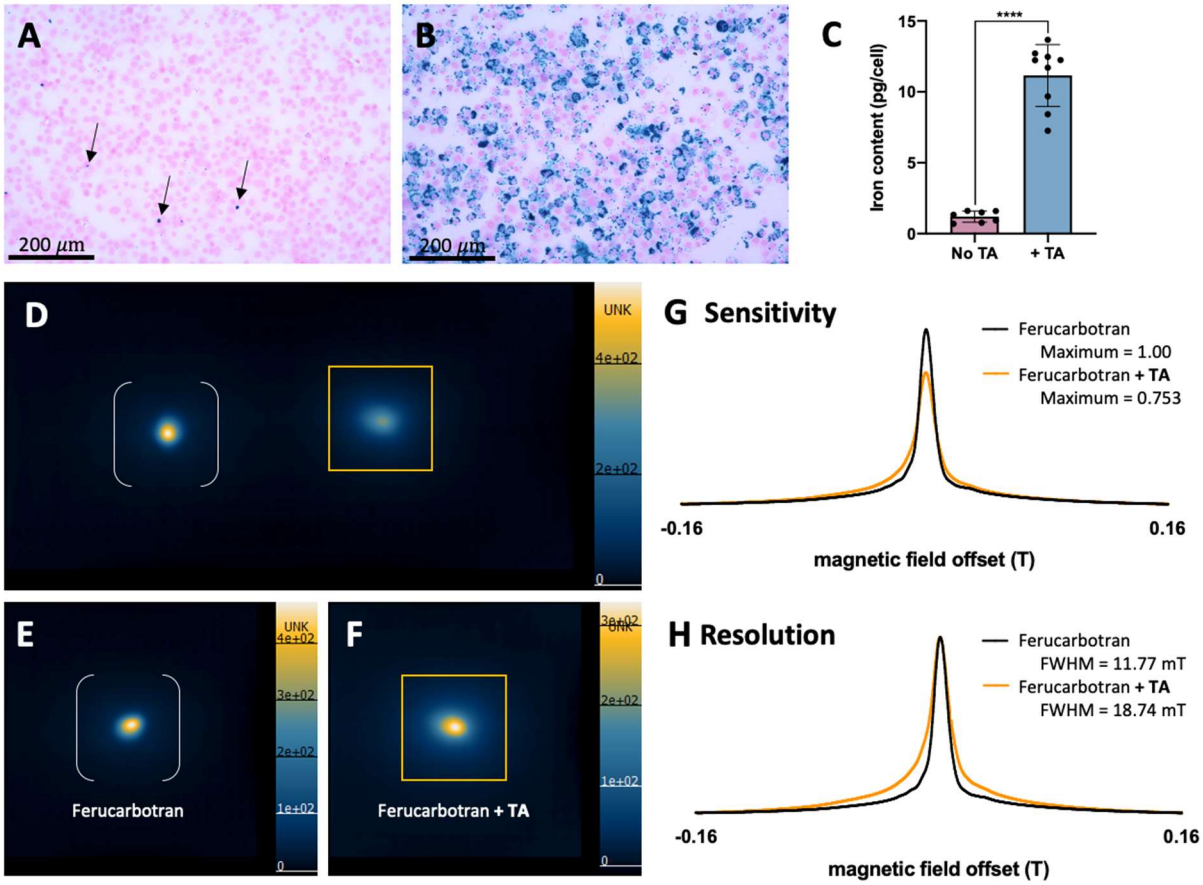

Figure 3 – The effect of transfection agents on cell labeling and MPI signal. Mesenchymal stem cells (MSC) labeled with ferucarbotran shows sparce and non-uniform labeling (denoted by black arrows) **(A)** wheras TA protamine sulfate and heparin improve this uptake of ferucarbotran **(B)** as shown with PPB stain. ICP-MS measurement of iron content (pg) per cell quantifies improved uptake of ferucarbotran in MSC using TA (**** $p < 0.0001$) **(C)**. MPI of 27.5 ug ferucarbotran alone **(white brackets in D and E)** and 27.5 ug ferucarbotran with TAs **(orange box in D and F)** show different MPI features. MPI images are displayed in full-dynamic range. As demonstrated in PSFs, the addition of TAs to ferucarbotran decrease MPI sensitivity **(G)** and worsens resolution **(H)** by changing SPION relaxation characteristics. Defined acronyms: MSC = Mesenchymal stem cell, PPB – Perl's Prussian blue, ICP-MS = inductively coupled plasma mass spectrometry, TA – transfection agent(s), FWHM = full width half maximum

Preprints (www.preprints.org) | NOT PEER-REVIEWED | Posted: 29 September 2020 doi:10.20944/preprints202009.0720.v1

Quantification of Cell Number

The ability to quantify cell number from MPI images represents a significant improvement for *in vivo* cell tracking with SPIONs. MPI signal (and the associated iron content) scales linearly with the number of cells present (Figure 4A). We, and others, have previously described techniques to measure MPI signal from images and determine the iron content in a region of interest (ROI).[13,17,37,38,56,57] Briefly, MPI images are displayed in full-dynamic range and the signal is delinated at the FWHM by referencing a colour look-up table (CLUT). Total MPI signal for the ROI can be calculated by:

$$\text{MPI signal} = \text{Mean signal in ROI (A.U.)} * \text{ROI volume (mm}^3\text{)}$$

A calibration is required to convert measured MPI signal to iron content. The relationship between MPI signal and iron content can be determined by measuring MPI signal from sample(s) of known iron content. A single reference phantom may be included for calibration.[13,38] Construction of a *calibration line* (MPI signal versus iron content) using multiple iron samples (5-10) increases the accuracy of this measurement. These samples must be the same SPION (with similar iron content and similar volume) and the MPI images of these samples must be acquired using the same imaging parameters. Figure 4B shows MPI images and a calibration line made by our group for ferucarbotran.

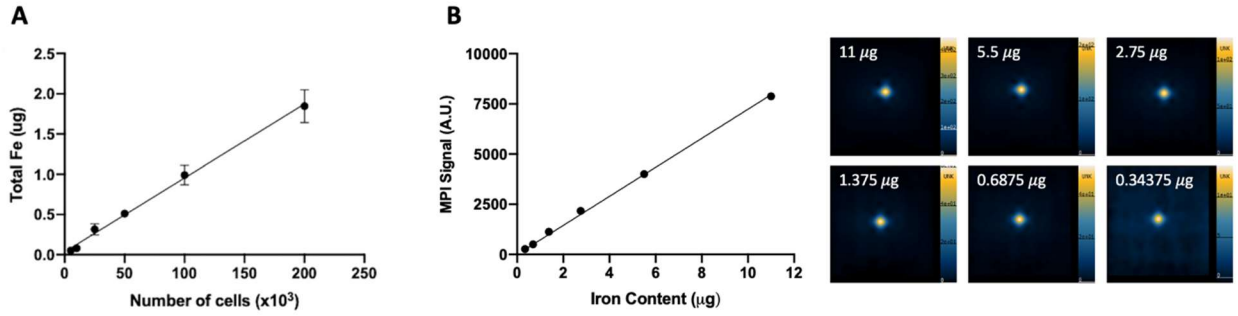

Figure 4 – MPI Quantification. The iron content measured from MPI images is directly linear with the number of ferucarbotran-labeled RAW 264.7 macrophages ($R^2 = 0.9789$) **(A)**. Reproduced from Makela et al. Molecular Imaging and Biology 2020. MPI signal is directly linear with the amount of iron, as displayed in a calibration line ($R^2 = 0.9969$) **(B)**. This line was produced by imaging multiple samples of ferucarbotran, which varied in iron mass, and the MPI signal from these images was quantified. MPI images are displayed in full-dynamic range.

The estimation of cell number from MPI images requires a measurement of cellular iron loading. For a sample prepared with a known number of cells, the average iron content per cell

Preprints (www.preprints.org) | NOT PEER-REVIEWED | Posted: 29 September 2020 doi:10.20944/preprints202009.0720.v1

can be measured using inductively coupled mass spectrometry (ICP-MS), spectrophotometry, or MPI. These measurements must be acquired using the same cells used for the *in vivo* imaging experiment. Subsequently, an estimation of cell number from *in vivo* MPI images can be calculated:

$$Number\ of\ cells\ in\ vivo = \frac{Measured\ iron\ content\ in\ vivo\ (by\ MPI)}{Measured\ iron\ content\ from\ cells\ in\ vitro\ (by\ MPI\ or\ ICP-MS)} * (Number\ of\ cells\ in\ vitro)$$

Caution/Challenges in the Quantification and Interpretation of MPI Data

When interpreting measurements of cell number from MPI images it is important to consider factors related to cell labeling which introduce uncertainty. First, the value for iron/cell measured from cell samples is an average value, some cells will contain more iron, some less. Second, the amount of iron/cell achieved with each cell labeling experiment has a range of values, even for the same labeling protocol, depending on precise timing and culture conditions. Uniform SPION labeling is optimal for cell tracking but is difficult to achieve. Magnetic sorting of cells is one strategy to improve the uniformity of labeled cells but this only removes those cells with low amounts of iron.

There are also factors which may impact the quantification of cell number over time. As cells proliferate *in vivo*, SPIONs are diluted between cell progeny leading to underestimation of cell number and potential loss of cellular detection over time by MPI[4,58]. Several studies have demonstrated that cells which are nonproliferative, or slowly proliferating *in vivo*, for example stem cells, can be monitored over longer periods of time.[13,30,36,39] When SPION-labeled cells undergo apoptosis *in vivo*, they are taken up by phagocytes for clearance by the liver.[4,39] This leads to diminished MPI signal at transplant sites;[36,37] the measurement of MPI signal in the liver can be used to provide a measure of labeled dead cells.[13,18,39] In the interim, bystander labeling of phagocytes may contribute to false MPI at the site of apoptosis. Lastly, the intracellular SPIONs which exist within endosomal compartments may be susceptible to degradation by lysosomes.[59,60] This degradation process can reduce the paramagnetism of iron oxide nanoparticles thereby altering their cellular MPI detectability.[61,62] This is a largely understudied phenomenon; however,

 doi:10.20944/preprints202009.0720.v1

it may be reasonable to assume that this effect depends on the biological inertness of the SPION and cellular lysosomal capacity.

When two sources of MPI signal are in close proximity, and are generated from tissues or samples which contain very different iron levels, the detection and quantification of the lower MPI signal can be challenging. This is illustrated in Figure 5. Here, cell pellets of bone-marrow dendritic cells (BMDCs) labeled with ferucarbotran containing $2.5x10^4$ or $5.0x10^5$ cells were imaged at a distance of 2 cm apart. Samples with equal numbers of SPION-labeled cells could be discerned but when the $5.0x10^4$ cell sample is imaged alongside the $2.5x10^4$ cell sample the MPI signal from the sample with fewerr cells (or, less iron) is hidden by the strong signal from the sample with more cells. This presents a major challenge for studies where the location of MPI signal is unknown, particularly for in-vivo cell tracking. Proposed solutions for overcoming this challenge include increasing gradient strengths for improved resolution, or using post-processing imaging techniques such as deconvolution filters. This requires further investigation, but is an important consideration for improving cell detection limits.

Preprints (www.preprints.org) | NOT PEER-REVIEWED | Posted: 29 September 2020 doi:10.20944/preprints202009.0720.v1

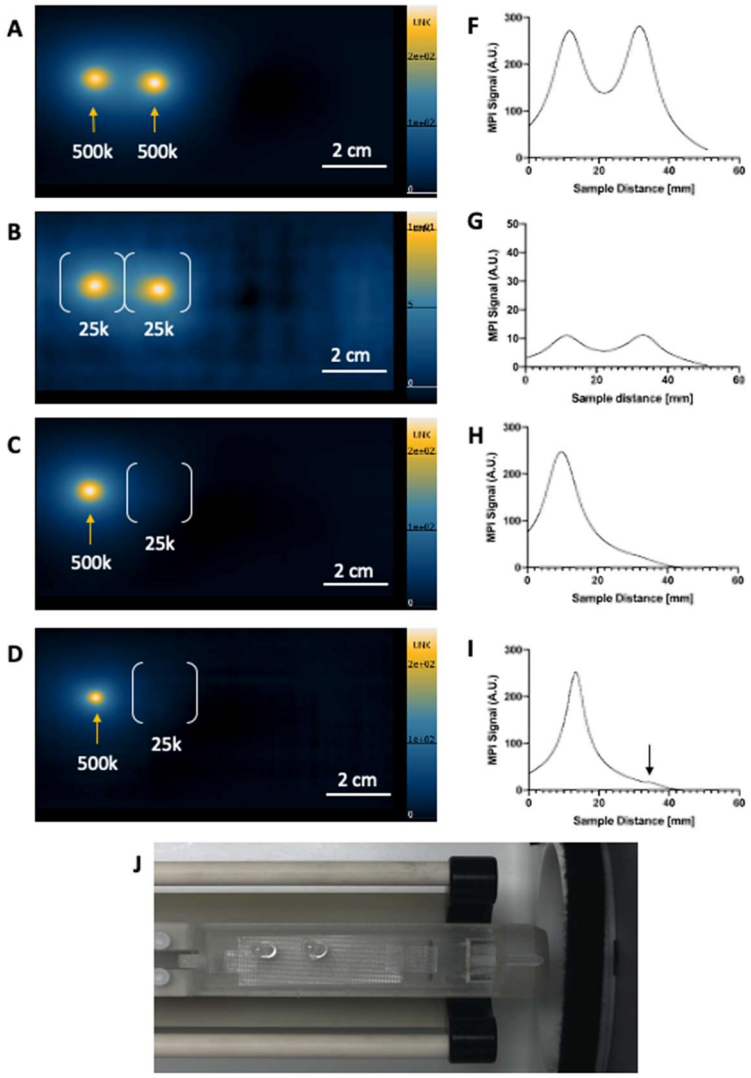

Figure 5 – MPI signal from low iron samples can be concealed by nearby high iron samples. Bone-marrow derived dendritic cells were labeled with ferucarbotran. Two identical samples of 500 x 10^3 cells (orange arrows) **(A)** and 25 x 10^3 cells (white brackets) **(B)** with 2 cm separation are visible and can be resolved in MPI images using low gradient strengths (3.0 T/m). However, the placement of 500 x 10^3 cells adjacent to 25 x 10^3 cells limits the detection of 25 x 10^3 cells using 3.0 T/m gradients **(C)** and 6.1 T/m gradients **(D).** MPI images are displayed in full-dynamic range. The corresponding signal intensity profiles are shown **(E-I)**. MPI signal cannot be resolved when samples were not identical **(H,I)**, however increased gradient strength (6.1T/m) helps to improve the detection of the 25 x 10^3 cell sample **(**black arrow, **I)**. A photograph of the imaging bed is shown with two cell sample holders **(J)**.

This issue can also arise from unwanted sources of MPI signal. For example, MPI signal is sometimes detected in regions of the digestive system of mice, owing to the presence of iron in mouse feed (Figure 1C) or at injection sites in mice, resulting from dried blood in the form of hemosiderin (unpublished results). Both of these MPI signal artifacts can be present in mice when no SPION labeled cells are present. If they are close to, or colocalize with, SPION-labeled cells it can be challenging to detect the region of interest.

 doi:10.20944/preprints202009.0720.v1

Conclusions

We are excited by the prospects of cell tracking with MPI. By combining the advantages of particle (SPION) sensitivity and signal specificity, prominent image contrast, and direct quantification, MPI has unique advantages over existing cell tracking modalities. Improvements in cellular sensitivity are expected from SPION development and cellular uptake strategies, which may help to advance towards the detection of single cells (or just say, a small number of cells). Yet there are still many aspects related to the interpretation of cell fate from MPI images which require improvements. These may provide exciting avenues for further investigation. Ultimately, we anticipate that cell tracking with MPI will contribute to our understanding of cellular therapies and guide therapeutic optimization.

1. Förster R, Braun A, Worbs T. Lymph node homing of T cells and dendritic cells via afferent lymphatics. *Trends Immunol*. 2012;33(6):271-280. doi:10.1016/j.it.2012.02.007

2. MartIn-Fontecha A, Sebastiani S, Höpken UE, et al. Regulation of dendritic cell migration to the draining lymph node: impact on T lymphocyte traffic and priming. *J Exp Med*. 2003;198(4):615-621. doi:10.1084/jem.20030448

3. Wang B, Sun C, Wang S, et al. Mouse dendritic cell migration in abdominal lymph nodes by intraperitoneal administration. *Am J Transl Res*. 2018;10(9):2859-2867.

4. Makela AV, Murrell DH, Parkins KM, Kara J, Gaudet JM, Foster PJ. Cellular imaging with MRI. *Top Magn Reson Imaging*. 2016;25(5):177–186.

5. Bulte JWM, Kraitchman DL. Iron oxide MR contrast agents for molecular and cellular imaging. *NMR Biomed*. 2004;17(7):484-499. doi:10.1002/nbm.924

6. Sykova E, Jendelova P. In vivo tracking of stem cells in brain and spinal cord injury. *Prog Brain Res*. 2007;161:367-383. doi:10.1016/S0079-6123(06)61026-1

7. Gonzalez-Lara LE, Xu X, Hofstetrova K, et al. The use of cellular magnetic resonance imaging to track the fate of iron-labeled multipotent stromal cells after direct transplantation in a mouse model of spinal cord injury. *Mol Imaging Biol*. 2011;13(4):702-711. doi:10.1007/s11307-010-0393-y

8. Hinds KA, Hill JM, Shapiro EM, et al. Highly efficient endosomal labeling of progenitor and stem cells with large magnetic particles allows magnetic resonance imaging of single cells. *Blood*. 2003;102(3):867-872. doi:10.1182/blood-2002-12-3669

9. Rivera-Rodriguez A, Hoang-Minh LB, Chiu-Lam A, et al. Tracking Adoptive T Cell Therapy Using Magnetic Particle Imaging. *bioRxiv*. Published online June 3, 2020:2020.06.02.128587. doi:10.1101/2020.06.02.128587

10. Zhang X, de Chickera SN, Willert C, et al. Cellular magnetic resonance imaging of monocyte-derived dendritic cell migration from healthy donors and cancer patients as assessed in a scid mouse model. *Cytotherapy*. 2011;13(10):1234-1248. doi:10.3109/14653249.2011.605349

11. de Chickera S, Willert C, Mallet C, Foley R, Foster P, Dekaban GA. Cellular MRI as a suitable, sensitive non-invasive modality for correlating in vivo migratory efficiencies of different dendritic cell populations with subsequent immunological outcomes. *Int Immunol*. 2012;24(1):29-41. doi:10.1093/intimm/dxr095

12. Jirak D, Kriz J, Strzelecki M, et al. Monitoring the survival of islet transplants by MRI using a novel technique for their automated detection and quantification. *Magma N Y N*. 2009;22(4):257-265. doi:10.1007/s10334-009-0172-4

13. Wang P, Goodwill PW, Pandit P, et al. Magnetic particle imaging of islet transplantation in the liver and under the kidney capsule in mouse models. *Quant Imaging Med Surg*. 2018;8(2):114-122. doi:10.21037/qims.2018.02.06

14. Heyn C, Ronald JA, Ramadan SS, et al. In vivo MRI of cancer cell fate at the single-cell level in a mouse model of breast cancer metastasis to the brain. *Magn Reson Med Off J Int Soc Magn Reson Med*. 2006;56(5):1001–1010.

15. Heyn C, Ronald JA, Mackenzie LT, et al. In vivo magnetic resonance imaging of single cells in mouse brain with optical validation. *Magn Reson Med*. 2006;55(1):23-29. doi:10.1002/mrm.20747

16. Fink C, Gaudet JM, Fox MS, et al. 19F-perfluorocarbon-labeled human peripheral blood mononuclear cells can be detected in vivo using clinical MRI parameters in a therapeutic cell setting. *Sci Rep*. 2018;8(1):590. doi:10.1038/s41598-017-19031-0

17. Gaudet JM, Ribot EJ, Chen Y, Gilbert KM, Foster PJ. Tracking the Fate of Stem Cell Implants with Fluorine-19 MRI. *PLOS ONE*. 2015;10(3):e0118544. doi:10.1371/journal.pone.0118544

18. Chapelin F, Capitini CM, Ahrens ET. Fluorine-19 MRI for detection and quantification of immune cell therapy for cancer. *J Immunother Cancer*. 2018;6(1):105. doi:10.1186/s40425-018-0416-9

19. Kadayakkara DKK, Janjic JM, Pusateri LK, Young W-B, Ahrens ET. In vivo observation of intracellular oximetry in perfluorocarbon-labeled glioma cells and chemotherapeutic response in the CNS using fluorine-19 MRI. *Magn Reson Med*. 2010;64(5):1252-1259. doi:10.1002/mrm.22506

20. Ahrens ET, Flores R, Xu H, Morel PA. In vivo imaging platform for tracking immunotherapeutic cells. *Nat Biotechnol*. 2005;23(8):983-987. doi:10.1038/nbt1121

21. Bulte JWM. Superparamagnetic iron oxides as MPI tracers: A primer and review of early applications. *Adv Drug Deliv Rev*. 2019;138:293-301. doi:10.1016/j.addr.2018.12.007

22. Zheng B, Yu E, Orendorff R, et al. Seeing SPIOs Directly In Vivo with Magnetic Particle Imaging. *Mol Imaging Biol*. 2017;19(3):385-390. doi:10.1007/s11307-017-1081-y

23. Lu K, Goodwill PW, Saritas EU, Zheng B, Conolly SM. Linearity and shift invariance for quantitative magnetic particle imaging. *IEEE Trans Med Imaging*. 2013;32(9):1565-1575. doi:10.1109/TMI.2013.2257177

24. Saritas EU, Goodwill PW, Croft LR, et al. Magnetic particle imaging (MPI) for NMR and MRI researchers. *J Magn Reson San Diego Calif 1997*. 2013;229:116-126. doi:10.1016/j.jmr.2012.11.029

25. Wu XLC, Zhang XY, Steinberg XG, et al. A review of magnetic particle imaging and perspectives on neuroimaging. *Am J Neuroradiol*. 2019;40(2):206-212. doi:10.3174/ajnr.A5896

26. Yu EY, Bishop M, Zheng B, et al. Magnetic Particle Imaging: A Novel in Vivo Imaging Platform for Cancer Detection. *Nano Lett*. 2017;17(3):1648-1654. doi:10.1021/acs.nanolett.6b04865

27. Wu LC, Zhang Y, Steinberg G, et al. A Review of Magnetic Particle Imaging and Perspectives on Neuroimaging. *Am J Neuroradiol*. 2019;40(2):206-212. doi:10.3174/ajnr.A5896

28. Talebloo N, Gudi M, Robertson N, Wang P. Magnetic Particle Imaging: Current Applications in Biomedical Research. *J Magn Reson Imaging*. 2020;51(6):1659-1668. doi:10.1002/jmri.26875

29. Tay ZW, Hensley DW, Chandrasekharan P, Zheng B, Conolly SM. Optimization of Drive Parameters for Resolution, Sensitivity and Safety in Magnetic Particle Imaging. *IEEE Trans Med Imaging*. 2020;39(5):1724-1734. doi:10.1109/TMI.2019.2957041

30. Zheng B, Vazin T, Goodwill PW, et al. Magnetic Particle Imaging tracks the long-term fate of in vivo neural cell implants with high image contrast. *Sci Rep*. 2015;5:14055. doi:10.1038/srep14055

31. Song G, Chen M, Zhang Y, et al. Janus Iron Oxides @ Semiconducting Polymer Nanoparticle Tracer for Cell Tracking by Magnetic Particle Imaging. *Nano Lett*. 2018;18(1):182-189. doi:10.1021/acs.nanolett.7b03829

32. Arami H, Ferguson RM, Khandhar AP, Krishnan KM. Size-dependent ferrohydrodynamic relaxometry of magnetic particle imaging tracers in different environments. *Med Phys*. 2013;40(7):1-14. doi:10.1118/1.4810962

33. Tay ZW, Hensley DW, Vreeland EC, Zheng B, Conolly SM. The Relaxation Wall: Experimental Limits to Improving MPI Spatial Resolution by Increasing Nanoparticle Core size. *Biomed Phys End Express*. 2017;3(3):1-21. doi:10.1088/2057-1976/aa6ab6.The

34. Chandrasekharan P, Tay ZW, Zhou XY, et al. A perspective on a rapid and radiation-free tracer imaging modality, magnetic particle imaging, with promise for clinical translation. *Br J Radiol*. 2018;91(1091). doi:10.1259/bjr.20180326

35. Tay ZW, Conolly SM. Order-of-magnitude resolution and SNR improvement using positive feedback MNP chains in magnetic particle imaging. *World Mol Imaging Congr*. Published online 2019.

36. Nejadnik H, Pandit P, Lenkov O, Lahiji AP, Yerneni K, Daldrup-Link HE. Ferumoxytol Can Be Used for Quantitative Magnetic Particle Imaging of Transplanted Stem Cells. *Mol Imaging Biol*. 2019;21(3):465-472. doi:10.1007/s11307-018-1276-x

37. Sehl OC, Makela AV, Hamilton AM, Foster PJ. Trimodal Cell Tracking In Vivo: Combining Iron- and Fluorine-Based Magnetic Resonance Imaging with Magnetic Particle Imaging to Monitor the Delivery of Mesenchymal Stem Cells and the Ensuing Inflammation. *Tomogr Ann Arbor Mich*. 2019;5(4). doi:10.18383/j.tom.2019.00020

38. Makela AV, Gaudet JM, Schott MA, Sehl OC, Contag CH, Foster PJ. Magnetic Particle Imaging of Macrophages Associated with Cancer: Filling the Voids Left by Iron-Based Magnetic Resonance Imaging. *Mol Imaging Biol*. 2020;22(4):958-968. doi:10.1007/s11307-020-01473-0

39. Zheng B, von See MP, Yu E, et al. Quantitative Magnetic Particle Imaging Monitors the Transplantation, Biodistribution, and Clearance of Stem Cells In Vivo. *Theranostics*. 2016;6(3):291-301. doi:10.7150/thno.13728

40. Bulte JWM, Walczak P, Janowski M, et al. Quantitative "Hot Spot" Imaging of Transplanted Stem Cells using Superparamagnetic Tracers and Magnetic Particle Imaging (MPI). *Tomogr Ann Arbor Mich*. 2015;1(2):91-97. doi:10.18383/j.tom.2015.00172

41. Gaudet J, Mansfield J, Goodwill P. Imaging Cancer Immunology: Tracking Immune Cells in vivo with Magnetic Particle Imaging. *J Immunol*. 2019;202(1 Supplement):130.7-130.7.

42. Eberbeck D, Dennis CL, Huls NF, Krycka KL, Gruttner C, Westphal F. Multicore Magnetic Nanoparticles for Magnetic Particle Imaging. *IEEE Trans Magn*. 2013;49(1):269-274. doi:10.1109/TMAG.2012.2226438

43. Yoshida T, Othman NB, Enpuku K. Characterization of magnetically fractionated magnetic nanoparticles for magnetic particle imaging. *J Appl Phys*. 2013;114(17):173908. doi:10.1063/1.4829484

44. Ferguson RM, Minard KR, Krishnan KM. Optimization of nanoparticle core size for magnetic particle imaging. *J Magn Magn Mater*. 2009;321(10):1548-1551. doi:10.1016/j.jmmm.2009.02.083

45. Houston WV. A Compound Interferometer for Fine Structure Work. *Phys Rev*. 1927;29(3):478-484. doi:10.1103/PhysRev.29.478

46. Mailänder V, Lorenz MR, Holzapfel V, et al. Carboxylated Superparamagnetic Iron Oxide Particles Label Cells Intracellularly Without Transfection Agents. *Mol Imaging Biol*. 2008;10(3):138-146. doi:10.1007/s11307-007-0130-3

47. Tang KS, Shapiro EM. Enhanced magnetic cell labeling efficiency using –NH2 coated MPIOs. *Magn Reson Med*. 2011;65(6):1564-1569. doi:10.1002/mrm.22843

48. Arbab AS, Bashaw LA, Miller BR, et al. Characterization of Biophysical and Metabolic Properties of Cells Labeled with Superparamagnetic Iron Oxide Nanoparticles and Transfection Agent for Cellular MR Imaging. *Radiology*. 2003;229(3):838-846. doi:10.1148/radiol.2293021215

49. Frank JA, Miller BR, Arbab AS, et al. Clinically Applicable Labeling of Mammalian and Stem Cells by Combining Superparamagnetic Iron Oxides and Transfection Agents. *Radiology*. 2003;228(2):480-487. doi:10.1148/radiol.2281020638

50. Bryant LH, Kim SJ, Hobson M, et al. Physicochemical characterization of ferumoxytol, heparin and protamine nanocomplexes for improved magnetic labeling of stem cells. *Nanomedicine Nanotechnol Biol Med*. 2017;13(2):503-513. doi:10.1016/j.nano.2016.07.011

51. Tang X, Loc WS, Dong C, et al. The use of nanoparticulates to treat breast cancer. *Nanomed*. 2017;12(19):2367-2388. doi:10.2217/nnm-2017-0202

52. Arbab AS, Bashaw LA, Miller BR, Jordan EK, Bulte JWM, Frank JA. Intracytoplasmic tagging of cells with ferumoxides and transfection agent for cellular magnetic resonance imaging after cell transplantation: methods and techniques. *Transplantation*. 2003;76(7):1123–1130. doi:10.1097/01.TP.0000089237.39220.83

53. Thu MS, Bryant LH, Coppola T, et al. Self-assembling nanocomplexes by combining ferumoxytol, heparin and protamine for cell tracking by magnetic resonance imaging. *Nat Med*. 2012;18(3):463-467. doi:10.1038/nm.2666

54. Buul GM van, Farrell E, Kops N, et al. Ferumoxides–protamine sulfate is more effective than ferucarbotran for cell labeling: implications for clinically applicable cell tracking using MRI. *Contrast Media Mol Imaging*. 2009;4(5):230-236. doi:10.1002/cmmi.289

55. Rughetti A, Biffoni M, Sabbatucci M, et al. Transfected human dendritic cells to induce antitumor immunity. *Gene Ther*. 2000;7(17):1458-1466. doi:10.1038/sj.gt.3301266

56. Parkins KM, Melo KP, Ronald JA, Foster PJ. Visualizing tumour self-homing with magnetic particle imaging. *bioRxiv*. Published online February 19, 2020:2020.02.17.953232. doi:10.1101/2020.02.17.953232

57. Melo KP, Makela AV, Hamilton AM, Foster PJ. Development of Magnetic Particle Imaging (MPI) for Cell Tracking and Detection. *bioRxiv*. Published online July 13, 2020:2020.07.12.197780. doi:10.1101/2020.07.12.197780

58. Ahrens ET, Bulte JWM. Tracking immune cells in vivo using magnetic resonance imaging. *Nat Rev Immunol*. 2013;13(10):755-763. doi:10.1038/nri3531

59. Golovko DM, Henning T, Bauer JS, et al. Accelerated stem cell labeling with ferucarbotran and protamine. *Eur Radiol*. 2010;20(3):640-648. doi:10.1007/s00330-009-1585-1

60. Toth GB, Varallyay CG, Horvath A, et al. Current and potential imaging applications of ferumoxytol for magnetic resonance imaging. *Kidney Int*. 2017;92(1):47-66. doi:10.1016/j.kint.2016.12.037

61. Suzuka H, Mimura A, Inaoka Y, Murase K. Magnetic Nanoparticles in Macrophages and Cancer Cells Exhibit Different Signal Behavior on Magnetic Particle Imaging. *J Nanosci Nanotechnol*. 2019;19(11):6857-6865. doi:10.1166/jnn.2019.16619

62. Guzy J, Chakravarty S, Buchanan F, et al. Complex Relationship Between Signal Intensity Properties in Magnetic Particle Imaging (MPI) and Iron Oxide Nanoparticle Degradation. Published online February 19, 2020. doi:10.26434/chemrxiv.11845584.v2